Neurochemical Research
https://doi.org/10.1007/s11064-022-03538-8

REVIEW

In Vivo ^{13}C Magnetic Resonance Spectroscopy for Assessing Brain Biochemistry in Health and Disease

Pravat K. Mandal[1,2] · Rimil Guha Roy[1] · Avantika Samkaria[1] · Joseph C. Maroon[3] · Yashika Arora[1]

Received: 9 August 2021 / Revised: 15 January 2022 / Accepted: 19 January 2022

Abstract

Magnetic resonance spectroscopy (MRS) is a non-invasive technique that contributes to the elucidation of brain biochemistry. ^{13}C MRS enables the detection of specific neurochemicals and their neuroenergetic correlation with neuronal function. The synergistic outcome of ^{13}C MRS and the infusion of ^{13}C-labeled substrates provide an understanding of neurometabolism and the role of glutamate/gamma-aminobutyric acid (GABA) neurotransmission in diseases, such as Alzheimer's disease, schizophrenia, and bipolar disorder. Moreover, ^{13}C MRS provides a window into the altered flux rate of different pathways, including the tricarboxylic acid cycle (TCA) and the glutamate/glutamine/GABA cycle, in health and in various diseases. Notably, the metabolic flux rate of the TCA cycle often decreases in neurodegenerative diseases. Additionally, ^{13}C MRS can be used to investigate several psychiatric and neurological disorders as it directly reflects the real-time production and alterations of key brain metabolites. This review aims to highlight the chronology, the technological advancements, and the applications of ^{13}C MRS in various brain diseases.

Keywords Brain · Carbon-13 · Magnetic resonance spectroscopy · Methodology development · Metabolic flux · Brain diseases

Introduction

Magnetic Resonance Spectroscopy (MRS) is a non-invasive method widely used for the characterization of tissue and the determination of biological processes in the body [1, 2]. Since its first observation in the 1980s, in vivo MRS of the brain has developed rapidly [3], using different MRS-active nuclei like ^{1}H, ^{31}P, ^{19}F, ^{23}Na, and ^{13}C. Initially, proton (^{1}H) and phosphorus (^{31}P) MRS were intensively used to detect the concentrations of several metabolites such as choline, N-acetyl aspartate (NAA), creatine, inorganic phosphate, phosphodiesters etc. Apart from this, cerebral pH and concentrations of different neurotransmitters were also detected [4]. ^{13}C MRS has developed about 30 years ago and since then it has provided more convenient diagnostic information as compared to ^{1}H, ^{31}P, etc. [5]. The uniqueness of ^{13}C MRS is its distinctive chemical specificity, permitting detection and quantification of metabolites that were not monitored by more conventional radiochemical techniques like positron emission tomography (PET) [6, 7]. Even though PET can provide critical information regarding regional cerebral glucose uptake after infusion of radiolabelled tracer [8, 9], the exact mechanism pertaining to dynamic glucose metabolism remains to be fully elucidated [8–11]. In such situations, ^{13}C MRS can provide novel insights about neurochemical profiles, macromolecular interactions, and dynamic brain glucose metabolism [12]. This will in turn aid us in gaining a better understanding of the etiopathology of various neurological disorders and consequently develop novel therapies.

Even though the most widely used noninvasive technique to measure neurochemicals is ^{1}H MRS [2, 13] there are major drawbacks like low dispersion of signals and narrow

Rimil Guha Roy and Avantika Samkaria have contributed equally.

✉ Pravat K. Mandal
pravat.mandal@gmail.com; pravat@nbrc.ac.in; pravat.mandal@florey.edu.au

[1] Neuroimaging and Neurospectroscopy (NINS) Laboratory, National Brain Research Centre (NBRC), Gurgaon, India

[2] Florey Institute of Neuroscience and Mental Health, Melbourne School of Medicine Campus, Melbourne, Australia

[3] Department of Neurosurgery, University of Pittsburgh Medical School, Pittsburgh, PA, USA

Published online: 28 January 2022

chemical shift range (0–5 ppm) as well as the inability to detect flux rates of different metabolic pathways in vivo. In contrast, ^{13}C MRS has been designed as a noninvasive method for estimating glutamate (Glu) neurotransmission and cell-specific neuroenergetics in humans. It provides complementary and early diagnostic information despite its low abundance (1.1%) and low gyromagnetic ratio (Fig. 1a and 2) [5]. To address the problem of poor ^{13}C signal intensity due to low gyromagnetic ratio and less abundant NMR active ^{13}C nuclei, advanced coils (dual tuned) are available (Fig. 1b). ^{1}H MRS detects Glu and glutamine (Gln) peaks as an overlapped peak and the combined concentration of the two neurometabolites is referred to as Glx. On the other hand, ^{13}C MRS discretely identifies these Glu, and Gln peaks, and the concentration of both has been unambiguously reported in various neurological diseases [14–16] (Fig. 3). Additionally, ^{13}C MRS detects diverse metabolic pathways in vivo upon the infusion of labeled substrates [5, 16, 17]. Large ^{13}C chemical shift dispersion (> 200 ppm) and distinctive chemical specificity make it an ideal technique to identify neurometabolites without any ambiguity [6, 7]. The pulse sequence for ^{13}C MRS studies involves the use of nuclear Overhauser effect (NOE) and subsequent broadband decoupling (^{1}H channel) during ^{13}C signal acquisition. This helps immensely to improve the ^{13}C signal coming from low abundant neurotransmitters [18]. With the availability of high-field MR scanners, sensitive ^{13}C coil, and advanced MR pulse sequence, ^{13}C MRS can be applied extensively in clinical settings [1]. The chemical shift values for some biologically relevant compounds can be found in Table 1.

^{13}C-labeled substrates (e.g., [1, 6-^{13}C]-glucose, [2-^{13}C]-acetate) are used as tracers for measuring the continuous labeling of downstream metabolic products like [4-^{13}C]-Glu and [4-^{13}C]-Gln. Such studies have helped to establish the relationship between neuronal and other activities and also the modulation of neuroenergetics [19]. This further provides detailed insights into the glial/neuronal metabolic compartmentation—an important factor for neurotransmitter synthesis and recycling [5]. ^{13}C MRS has enabled studying in vivo cell-specific brain metabolism [20], especially in tumors [16], chronic hepatic encephalopathy (CHE) [14], Alzheimer's disease (AD) [15], and major depressive disorders (MDD) [21]. ^{13}C MRS is used to investigate the modulation of Glu neurotransmission, TCA cycle, glycolysis, pentose phosphate pathway, and N-acetyl aspartate synthesis.

In this review, we briefly discuss the ^{13}C MRS technique and their current applications in neuroscience research. This review presents the chronology, the technological

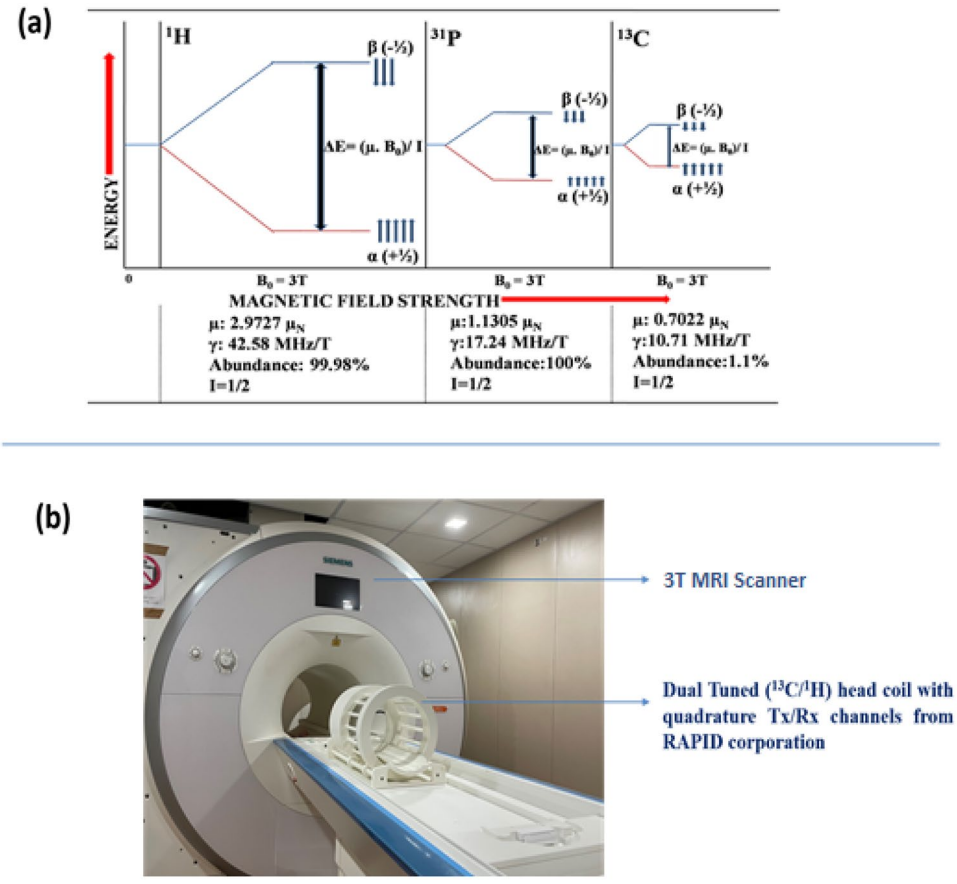

Fig. 1 **a** Comparison between the splitting of energy levels of ^{1}H, ^{31}P, and ^{13}C nuclei. In the presence of an external magnetic field (B_0), the energy levels split into α and β states. The difference between α and β depends on the magnetic moment (μ) [μ(^{1}H) > > μ(^{31}P) > μ(^{13}C)], resulting in the highest sensitivity for ^{1}H MRS, followed by ^{31}P MRS, and finally ^{13}C MRS (I, spin; γ, gyromagnetic ratio ($\frac{\mu}{I}$) MHz/T). Proportionality has been maintained considering the magnetic moment of the three nuclei in the figure. **b** Picture of 3 T Prisma MRI scanner (at NBRC) attached with dual tuned head coil from RAPID Corporation. The Tx/Rx ^{13}C coil is internally connected with multinuclear amplifier

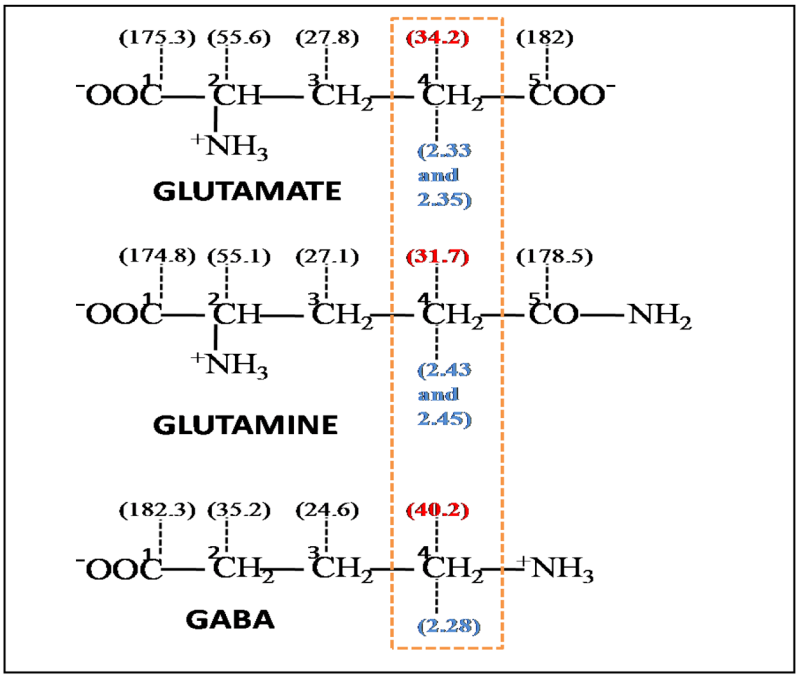

Fig. 2 Chemical shift values of ^{13}C MRS (red) and ^{1}H MRS (blue) of the major neurotransmitters and neurometabolites: glutamate, GABA, and glutamine for ^{1}H and ^{13}C MRS: Glu($4CH_2$) δ_H-2.33 and 2.35; δ_{13C}-34.2, Gln($4CH_2$) δ_H-2.43 and 2.45; δ_{13C}-31.7, GABA($4CH_2$) δ_H -2.28; δ_{13C}-40.2 ppm. Hence, due to the crowding of ^{1}H signals and peak overlapping, Glu and Gln peaks are referred as mixed Glx, while the metabolites are distinguishable at C4 position as evident from the ^{13}C MRS spectra

advancements, and the applications of ^{13}C MRS in various brain diseases. Outcomes from several studies are discussed to corroborate ^{13}C MRS methods and its possible applications in the study and diagnosis of neurological diseases. We have used PubMed, Google Scholar, and Web of Science to extract relevant articles from the year 1955 to 2021 for manuscript preparation.

Technological advancements of ^{13}C MRS

^{13}C MRS was initially applied to measure the distribution of ^{13}C metabolites from the abdominal region, head, calf muscle, and muscle glycogen levels in humans [22, 23]. The technological development of ^{13}C MRS technique and the associated hardware and processing software advancements have immensely improved the spatio-temporal resolution of spectral data [6]. This makes ^{13}C MRS a unique method to study neurotransmission and neuroenergetics noninvasively (Fig. 4) [24].

An initial study using ^{13}C MRS for the detection of neurometabolites employed a 1.5 T whole-body scanner [25]. Radiofrequency (RF) coils in ^{13}C MRS spectroscopy, however, pose a significant challenge due to the lower resonance frequency of ^{13}C nuclei. It is being used in the presence of existing ^{1}H coils for decoupling and NOE purposes. The broadband stochastic decoupling and WALTZ-8 pulse sequence are generally used for effective decoupling to generate improved signal-to-noise (SNR) ratio. The development of Image Selected In vivo Spectroscopy technique imparts better field homogeneity [26, 27], whereas upgraded WALTZ-16 decoupling pulse permits operations with much lower RF power [28]. Higher magnetic field strength scanners and gradient coils ease the detection of narrow (2–3 Hz) natural abundance signals from metabolites, including Glu, Myo-inositol, Gln, and N-acetyl-aspartate [29]. Pulse sequence PRoton Excited Carbon-13 Image SElected in vivo Localized spectroscopy (PRECISELY) provides the acquisition of naturally abundant brain glucose signals [30]. Quadrature hybrid coils made of two distinct RF channels efficiently separate ^{1}H (169 MHz) and ^{13}C (42.5 MHz) frequencies using a 4 T scanner. Heteronuclear Single Quantum Coherence (HQSC) resolves amide peaks without any ambiguity [31]. This enables multi-volume ^{1}H–^{13}C correlation spectroscopy to be used even on a whole-body scanner with ^{1}H sensitivity and superior metabolite resolution via ^{13}C chemical shift.

Progression in coil design leads to the creation of a quadrature transmit/receive head-coil optimized for ^{13}C MR sensitivity [32]. Recent advancements in low-power broadband proton stochastic decoupling pulse have enabled the use of a 7 T scanner for human studies [33]. This has greatly aided in the evaluation of the occipital cortex. The technological development of coils for better SNR has also become an active area of research to improve the quality of data for maintaining specific RF absorption rate (SAR) restriction [34]. Moreover, we previously developed a signal-processing user-friendly package KALPANA that can be used to provide standardized quantitation of

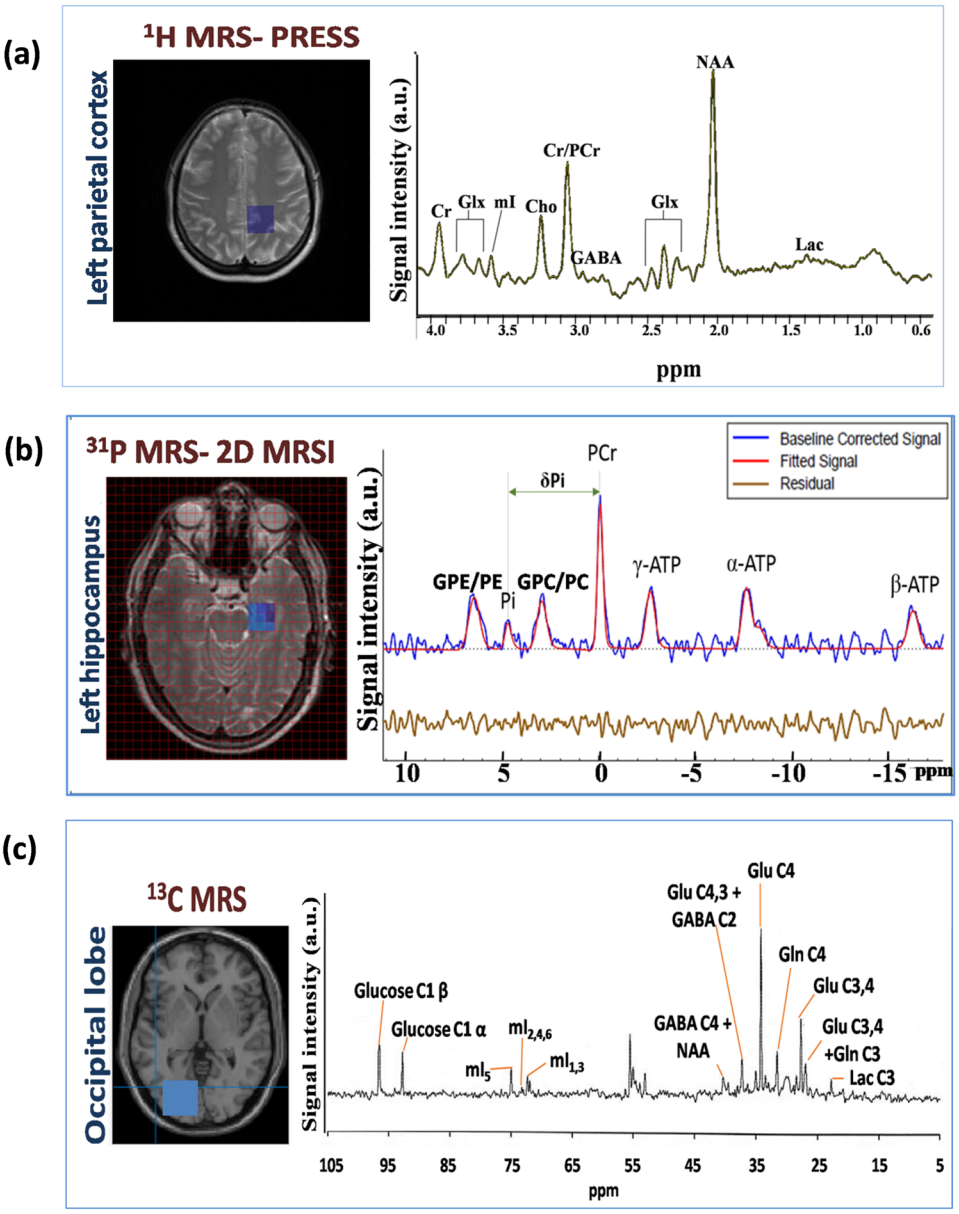

Fig. 3 Representative ^{1}H, ^{31}P, and ^{13}C MRS spectra from the brain. **a** ^{1}H MRS spectra showing the obtained Glu and Gln resonances that are non-separable and referred as a combined peak of Glu + Gln (Glx) due to the proximity and overlapping of peaks, **b** ^{31}P spectra detecting metabolites containing various phosphate moiety, and **c** ^{13}C MRS spectra depicting unambiguous chemical shift ^{13}C positions of GABA, Glu, and Gln at their labeled 4-CH_2 moiety after intravenous infusion of [1-^{13}C] glucose into a human subject. ^{1}H and ^{31}P MRS spectra have been acquired from the brain of a healthy adult using a 3 T (Philips at NBRC) scanner in **a** and **b**. ^{13}C MRS spectra reproduced with permission from the publisher [56], in **c** and voxel placements for the figures were performed for illustration purpose only

neurometabolites for identifying diagnostic biomarkers (^{1}H, ^{31}P, ^{19}F, ^{13}C, etc.) [35].

Physics Underlying ^{13}C MRS

The low gyromagnetic ratio and natural abundance of ^{13}C nuclei makes it difficult to obtain good signal intensity during a routine ^{13}C MRS experiment. Additionally, heteronuclear coupling between ^{1}H–^{13}C ($_{1}J_{CH}$ = 125–145 Hz) must be removed to obtain increased sensitivity of the ^{13}C MR measurement. To mitigate this problem, signal enhancement strategies must be employed. Usually, decoupling of ^{1}H-^{13}C scalar bonds is performed. Here, radio frequency power transmitted at the ^{1}H frequency during ^{13}C reception leads to decoupling of the ^{1}H-^{13}C bond and leads to a simplified spectral pattern and an increase in the carboxylic/amide ^{13}C signals by a factor of 4 [33, 36]. This is because of the integrated impacts of proton decoupling and NOE. ^{13}C MRS utilizes average transmit power and decoupling power of less than 3.6 W and 35 W, respectively. Utilizing the spectrum without decoupling and NOE, the peak amplitude of aspartate C1 (Asp1, 175.0 ppm) was escalated by a component of 2.3 when NOE was on, and by a component of 5.3 when decoupling and NOE both were on. Proton decoupling resolved the resonances of aspartate C1 (175.0 ppm) and glutamine C1 (Gln1, 174.8 ppm) as well as glutamine C5 (Glu5, 178.5 ppm) and aspartate C4 (Asp4, 178.3 ppm) [33]. The effect disappears as soon as the decoupling pulse is turned off; hence, decoupling irradiation must remain on during the acquisition. Two commonly employed decoupling

Table 1 ^{13}C MRS chemical shift values of biologically relevant compounds. Table has been adapted from [142]

Compound	Carbon atoms					
	C1	C2	C3	C4	C5	C6
Acetate	182.6	24.5				
Alanine	176.6	51.5	17.1			
Aspartate	175.1	53.2	37.4	178.4		
Bicarbonate	161.0					
Citrate	179.7	46.8	76.0	182.3	46.8	179.7
Creatine	175.4	37.8	158.0	54.7		
GABA	182.3	35.2	24.6	40.2		
Glycerol	63.1	72.8	63.1			
β-hydroxybutyrate	181.2	47.6	66.8	22.9		
Glucose α	92.7	72.1	73.5	70.4	72.1	61.4
Glucose β	96.6	79.9	76.5	70.4	76.5	61.4
Glutamate	175.3	55.6	27.8	34.2	182.0	
Glutamine	174.8	55.1	27.1	31.7	178.5	
Glycine	173.3	42.5				
Glycogen	100.5		74.0	78.1	72.1	61.4
Myo-inositol	73.3	73.1	73.3	71.9	75.1	71.9
Lactate	183.3	69.3	21.0			
Malate	182.1	71.7	43.9	180.9		
NAA	179.7	54.0	40.3	179.7	174.3	22.8
Succinate	183.4	35.3	35.3	183.4		
Taurine	48.4	36.2				

Fig. 4 Chronology of development pertaining to ^{13}C MRS technique in human studies. Since 2016, clinical studies have mainly utilized the technique of hyperpolarized ^{13}C MRS to probe into diseases like cancer

methods are continuous wave (CW) decoupling and broadband decoupling. There is a concurrent linear increase in the SAR with the duration of decoupling [37]. Due to the longer T1 relaxation time of ^{13}C nuclei, a longer time is needed to conduct a ^{13}C MRS experiment. This further increases the SAR load during an experiment due to the elongated time. International consortiums like the US Food and Drug Administration (FDA) and the International Electrotechnical Commission (IEC) have devised parameters to keep SAR levels within an acceptable range without causing harm to the subjects during a proton-decoupled ^{13}C MRS experiment. Developing RF pulses with better power and amplitude has since been an active area of research to keep up with the advent of high field clinical magnets [18, 37–39]. This will help in maintaining the SAR value below RF safety thresholds. An in-depth analysis of this, however, is beyond the scope of this review.

In order to minimize the contamination from the extracranial triglycerol resonance, spatial localization of the ^{13}C signal is crucial [40]. It also guarantees a certain proportion of anatomical specificity. Unfortunately, the huge chemical shift scattering of ^{13}C resonance leads to localization errors. The chemical shift displacement artefact (CSDA) is suggested to be proportional to difference in the carrier frequency and it is inversely proportional to spectral bandwidth. CSDA are much larger for ^{13}C MRS localization procedures than for ^{1}H MRS. CSDAs are most troublesome with single voxel spectra at higher magnetic fields and decreasing gradient strength. Additionally, they also depend on bandwidth i.e., the narrower the bandwidth, the more contamination is observed. The popular solution is to employ stronger imaging gradients and larger bandwidth RF pulses [41]. Contamination from extracranial lipids hampers the utilization of ^{1}H MRSI. There are a few accepted and emerging techniques for extracranial lipid suppression involving: (a) outer volume suppression (OVS) by saturating skull region with multi-slice excitation pulses; (b) cubical inner volume selection (IVS) which is based on STEAM, PRESS, etc.; (c) localization based on RF shimming; (d) T1-based nulling; (e) crusher coils [42]. Most of these methods are established on inversion recovery or spatially or spectrally selective excitation of the lipid signal which is followed by dephasing [43]. Recently, post-processing-based methods are gaining popularity because any additional RF pulses in the sequence are absent [42].

Cerebral Glucose Metabolism

Glucose enters the brain via GLUT1 receptors. In neurons, it is oxidized to pyruvate by glycolysis [37]. Pyruvate is either converted to lactate or undergoes decarboxylation. Decarboxylation incorporates pyruvate into tricarboxylic acid cycle (TCA), where it condenses irreversibly with oxaloacetate (OAA) to form citrate, which is further metabolized to α-ketoglutarate (α-KG). α-KG continues in the TCA cycle while a fraction of it gets transaminated to Glu (Fig. 5). The rate of α-KG/Glu exchange can be detected by ^{13}C MRS to investigate mitochondrial alteration [37, 44]. In a clinical study with AD patients, loss of ^{13}C labelling in C4 of glutamate indicated an impaired TCA cycle. The relation between mitochondrial dysfunction and neurodegenerative diseases may provide a

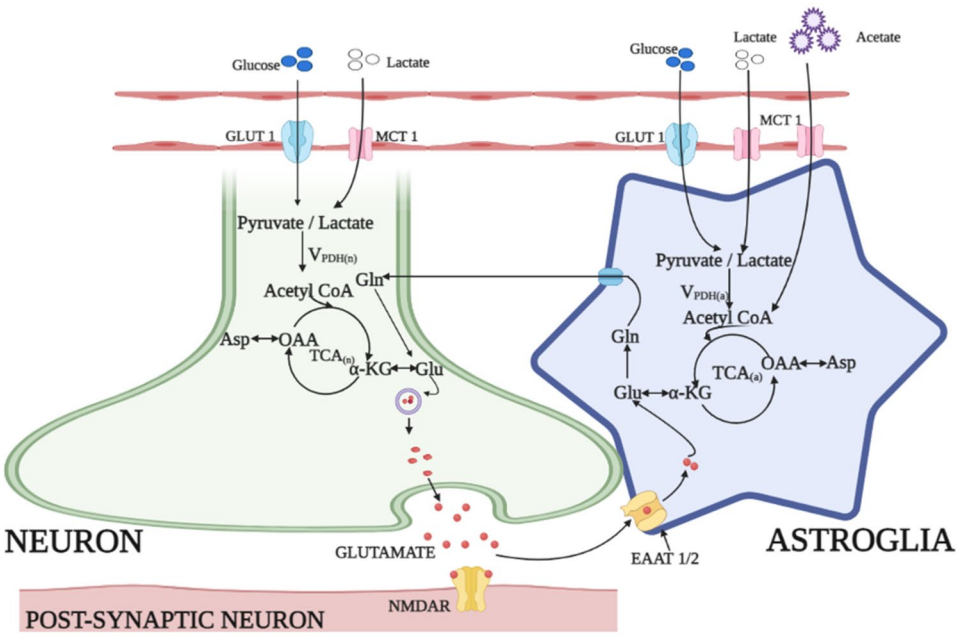

Fig. 5 Substrate entry and neurotransmitter cycle. Description of the entry and metabolism of glucose, lactose, and acetate in neurons and astroglial cells. Glucose and lactate are incorporated into neuronal and glial TCA cycle by the enzyme pyruvate dehydrogenase. Acetate is exclusively metabolized in astroglia. Following glutamate neurotransmission, excess glutamate in the synapse is taken up by astroglial Glu transporters and converted to Gln by glutamine synthetase. Gln is further synthesized in astroglia by either Glu/Gln cycle or de novo from pyruvate by PC. ^{13}C MRS helps in measuring the rates of these pathways by infusing ^{13}C labelled substrates. The figure is reproduced with permission from the publisher [24]

mechanistic link between such diseases and their psychiatric symptoms [5, 24].

Metabolism of ^{13}C Enriched Substrates

^{13}C MRS contributes to the understanding of cerebral metabolism and its correlation to neuronal activity by detecting metabolites labeled with ^{13}C-enriched substrates [24, 45–47]. This provides insight into the dynamic labeling and flux of various metabolic pathways, such as glycolysis, glycogenolysis, pentose phosphate pathway (PPP), gluconeogenesis, TCA cycle, and Glu-Gln/GABA cycle [47].

Glucose: [1-^{13}C]-glucose and [1, 6-$^{13}C_2$]-glucose are widely used in in vivo ^{13}C MRS studies. The incorporation of labels from [1-^{13}C]-glucose into [4-^{13}C]-Glu often reflects the neuronal glycolytic pathway and TCA cycle [45, 46]. In one study, the flux of the cerebral TCA cycle was measured in rat brains using ^{13}C isotope [48]. ^{13}C-labeled glucose undergoes glycolysis in the brain, wherein the label is transferred to [3-^{13}C] pyruvate, which further participates in TCA cycle. In the first turn of the cycle, α-KG_4 picks up the label, which is further picked up by and passed on to subsequent substrates (viz. Glu_4) via enzyme-mediated fast exchange. Studies have reported this flow of labels after 10–15-min infusion time (Fig. 6). Labeling patterns depend on the time course of the infusion of labeled substrates. With greater infusion times, more isotopomers get labeled in the succeeding steps of the cycle [46]. [2-^{13}C]-glucose can also be used to measure metabolic fluxes and provides additional sensitivity in measuring the flow of ^{13}C isotope through anaplerosis of Glu and astroglial TCA cycle. It leads to the enrichment of the astroglial pool of [3-^{13}C] Glu/Gln. [5-^{13}C] Glu/Gln labeling occurs by the action of pyruvate dehydrogenase. However, the C5 label is often lost in CO_2 evolution and only the C3-labelled pool of Glu/Gln accumulates, which is a direct measure of the anaplerotic rate of the astroglial TCA cycle [46].

Acetate: Studies suggest that acetate is exclusively metabolized in astroglia [46, 49]. As a substrate, [1, 2-^{13}C]-acetate or [2-^{13}C]-acetate is selectively transported in the astrocytes, and a small astroglial Glu pool (ranging 0.5–1.0 mM) is initially labeled. Subsequently, ^{13}C-labeled compound is transported from a large astroglial [4-^{13}C]-Gln pool to large neuronal Glu pool via the Glu/Gln cycle [46, 49, 50]. The co-infusion of glucose and acetate conducted in humans and rats has led to the measurement of both astroglial and neuronal metabolism through ^{13}C–^{13}C isotopomer resonances [5, 51]. Additionally, β-hydroxybutyrate and lactate have been used for infusion studies [52, 53]. β-hydroxybutyrate has proven to be a major substrate during prolonged fasting or when a person follows a ketogenic diet, and its metabolism pattern follows closely that of glucose [54].

^{13}C MRS is performed by administering labeled substrates or in natural abundance state. Labeled glucose is administered orally or intravenously to enrich the labeling pattern of metabolites and measure corresponding enzymatic fluxes and concentrations of several metabolites [55]. The labeling patterns of orally administered and IV-infused enriched glucose have been compared previously [56]. At isotopic steady state, spectra showed more scattering in case of orally administered glucose as compared to IV-infused glucose (Fig. 7). The labeling pattern after the infusion of ^{13}C-enriched substrates is also mentioned (Fig. 8).

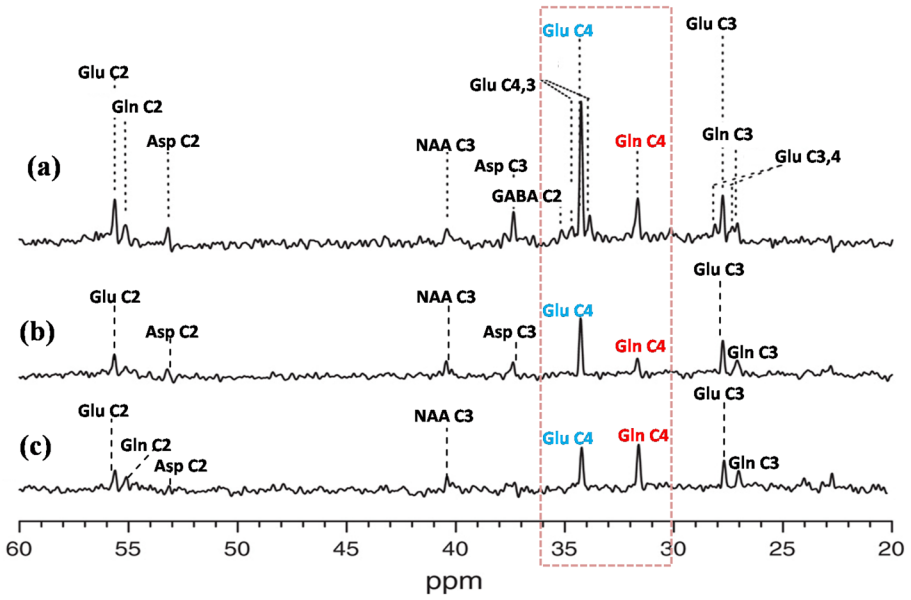

Fig. 6 Localized ^{13}C MRS spectra acquired from the occipital–parietal lobe of a healthy subject using a 4 T scanner after the infusion of **a** [1-^{13}C] glucose, **b** [3-^{13}C] lactate, and **c** [2-^{13}C] acetate. Spectra are scaled to NAA C3. The highest fractional enrichment of substrates was obtained after the infusion of labeled glucose as precursor. For glucose or lactate as labeled precursors, the label can be seen accumulating mostly in Glu C4. Acetate preferentially labels Gln C4, as it is preferentially metabolized in astrocytes. Figure reproduced with permission from the publisher [24]

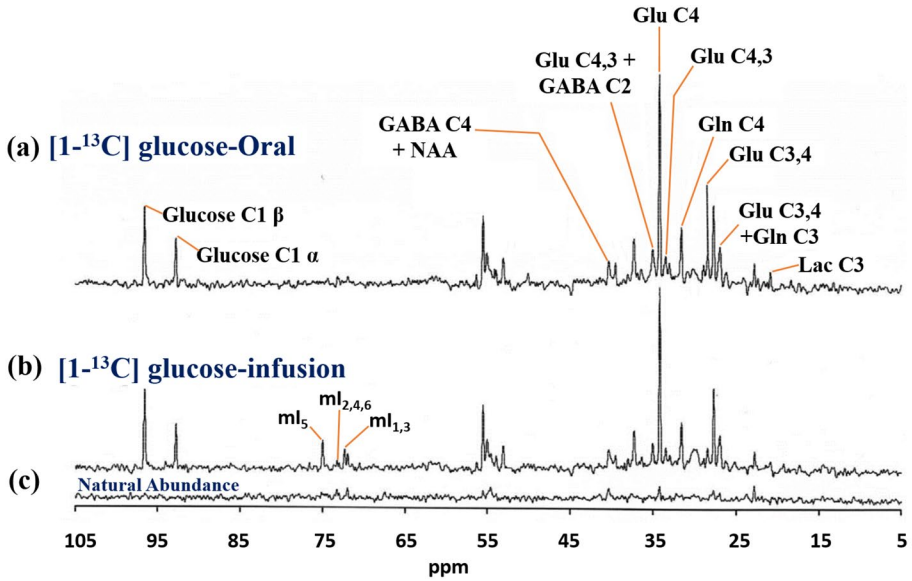

Fig. 7 Difference in spectra after oral and IV administration of labeled glucose. Spectra obtained from a healthy subject at natural abundance and after administering ^{13}C-labeled glucose (oral and infusion). Major metabolites, including Gln, Glu, GABA, and myo-inositol, have been detected. **a** Spectra acquired after oral administration. Presence of major metabolites is illustrated. However, the peaks of mI were absent. **b** Spectra after the infusion of [1-^{13}C] glucose intravenously. The peaks of mI are clearly distinguished. **c** Naturally abundant peaks without the substrate intake. The peak heights are highly diminished. Figure reproduced with permission from the publisher [56]

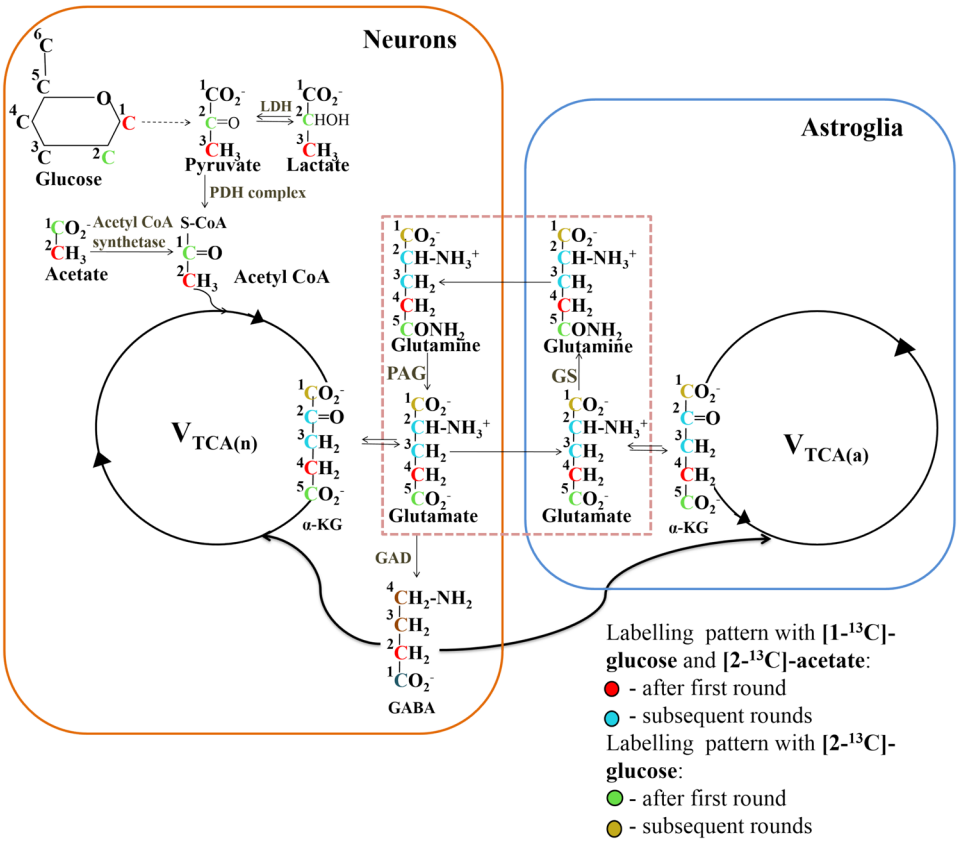

Fig. 8 Labeling pattern after the infusion of ^{13}C-enriched substrates. The sequential transfer of ^{13}C isotope can be noticed as the metabolic pathways ensue (α-KG α-ketoglutarate; GABA γ-aminobutyric acid; GAD Glutamic acid decarboxylase; PAG Phosphate-activated glutaminase; GS Glutamine synthetase). Figure reproduced with permission from the publisher [49]

Neurotransmitter Cycling and Neuroenergetics

The brain delimits many metabolic pathways and perturbations that can lead to neurodegenerative or neuropsychiatric disorders. Glu/Gln cycle is a regulator that helps understand neuronal energy metabolism. Derived from Glu, GABA also provides information regarding neurometabolism, and both cycles can be studied by ^{13}C MRS to detect neuronal metabolism and its correlation with neuroenergetics [57]. This helps compare neuronal and glial metabolism and establish the link between neuroenergetics and neurotransmitter cycling [24].

Glutamate–Glutamine Cycle and Its Linkage to Neuroenergetics

Glu is the major excitatory neurotransmitter released into the synapse by exocytosis from synaptic vesicles [58]. The excess Glu enters astrocytes to undergo either TCA cycle or the conversion to Gln by glutamine synthetase. In neurons, Gln is metabolized by phosphate-activated glutaminase back to Glu.

The presence of Glu/Gln cycle has been validated by studies depicting the localization of glutamine synthetase to the astrocytes and phosphate-activated glutaminase in the neurons [45, 47]. An early in vivo ^{13}C MRS study measured the rates of total Glu/Gln cycling ($V_{cyc\ (tot)}$) and neuronal glucose oxidation ($CMR_{glc\ (ox)\ n}$) [59]. Perturbations in these flux rates can be measured in different brain regions, including the hippocampus/dorsolateral pre-frontal cortex in AD, dementia, etc., to provide the impact of these diseases in affected anatomical locations. The relationship between neurotransmitter cycling and neuroenergetics can also be analyzed using electrophysiological techniques. In one study, cortical activity was modulated using carbon-fiber electrodes, and measurements of $V_{cyc(tot)}$ and $CMR_{glc(ox)n}$ were conducted on anesthetized rats at different levels of electrical activity [24, 57, 59, 60]. This demonstrated that for every round of the neurotransmitter cycle, one molecule of glucose is oxidized [57].

GABA–Glu Cycle and Its Linkage to Neuroenergetics

GABA is the major inhibitory neurotransmitter present in the brain. GABA is a resultant of Glu metabolism and acts synergistically with Glu to maintain the excitatory–inhibitory homeostasis in the brain [61, 62]. Alterations in GABA and/or Glu can induce neurological disorders. One ^{13}C nuclear magnetic resonance (NMR) study on rats reported that the transfer of labels by GABA catabolism to Gln_4 is not distinct from direct labeling by neuronal Glu_4 in Glu/Gln cycle [62]. The importance of GABAergic role in cerebral metabolism has been described by NMR studies [62]. One study evaluated the correlation of mitochondrial TCA cycle and neurotransmitter cycle fluxes with glutamatergic, GABAergic neurons, and astroglia in brain regions, including the cerebral cortex and hippocampus, of young and aged mice using ^{1}H–[^{13}C]–NMR spectroscopy in combination with timely infusion of ^{13}C-labeled glucose and acetate. The researchers reported a decrease in the excitatory–inhibitory neurotransmitter activity associated with GABAergic and glutamatergic neurons. This decrease was reported to be qualitatively associated with cognitive decline in aged mice [63].

Metabolic Modeling

The application of ^{13}C MRS using selective ^{13}C-enrichment pattern aids qualitative and quantitative studies on metabolic compartmentation and fluxes. Quantitative information regarding the concentration of specific metabolites is usually obtained through metabolic modeling. Metabolic models are computationally constructed using mathematical tools and algorithms to express the ^{13}C-labeling pattern of detected metabolites as a function of metabolic fluxes. Usually, multi-compartment models are used to quantify metabolic fluxes [64].

The simplest model is the one-compartment model. It takes into consideration only neurons to quantify flux rates from metabolic pathways. Metabolic modeling is usually performed after the administration of enriched substrates. It is essential to calculate isotopic enrichment, without which the rate of labeling cannot be properly derived [65].

Usually, an assumption of metabolic steady state is made on the basis of biochemical homeostasis of physiological systems. At such instances, the influx and efflux of metabolites resulting in the transfer of labels following mass conservation can be represented as follows (for two pools) [47]:

$$\frac{d[C]}{dt} = V_1 + V_2 - V_3$$

In this case, V_1 represents the rate of one pool, V_2 the rate of another pool, and C is the resultant of the two pools consumed at rate V_3 (in µmol/g/min). Since total influx is considered equal to total efflux,

$$V_3 = V_1 + V_2$$

The isotope balance equation can be written as:

$$\frac{d[C_{k^*}]}{dt} = V_1 \frac{[A_{i^*}]}{[A]} + V_2 \frac{[B_{j^*}]}{[B]} - (V_1 + V_2) \frac{[C_{k^*}]}{[C]}$$

where C_k^*, A_i^*, and B_j^* represent labeled products. Metabolic modeling for dynamic labeling allows the quantification of absolute flux from metabolic pathways with higher reliability. Depending upon the type of metabolic modeling

approach, differential equations can be constructed on the basis software, such as MATLAB. Monte–Carlo simulations can be performed to analyze the robustness and reliability of the model.

Cerebral Metabolic Compartmentation

Preliminary experiments regarding metabolic compartmentation in the brain involve injecting ^{13}C-Glu into the external occipital protuberance of Sprague–Dawley rats [66]. Several ^{15}N and ^{13}C tracer studies depict that Gln is more highly labeled than its metabolic precursor Glu, and two separate pools of Glu and Gln were discovered [47, 49]. Technological advancements in MRS have enabled in situ analysis of metabolic fluxes in the brain concerning different metabolic pathways [67, 68]. Studies on both human [25, 30, 67, 69] and animal brains [49, 50, 70–72] have reported cerebral metabolic compartmentation using ^{13}C-enriched substrates. The most popular models to calculate flux rates are two- and three-compartment models. In the two-compartment model, neurons and glia are considered separately, whereas, in the three-compartment model, neurons are subdivided into glutamatergic and GABAergic neurons to account for the flux rate of GABA–Glu–Gln cycle. Infusion of enriched substrates quantifies the rates of neuronal TCA cycle, glial TCA cycle, PC flux, and glutamatergic and GABAergic neurotransmission simultaneously through metabolic modeling approaches (as shown in Fig. 9) [47, 62, 73].

The figure depicts the transfer of labels after the infusion of [1-^{13}C]-glucose and [2-^{13}C]-acetate after only the first turn of TCA cycle. Using ^{13}C MRS, the cerebral metabolic rate can be calculated from various metabolic fluxes following the flow of labels using mathematical modeling. Figure is adapted with permission from the publisher [136]

^{13}C MRS in Clinical Setting

The technique of ^{13}C MRS has been applied in many clinical studies to probe neurochemical alterations as well metabolic abnormalities that arise in different brain diseases. Some applications of ^{13}C MRS for different clinical conditions are briefly discussed in this section to illustrate the state-of-the-art utility of the modality in clinical settings. In a study assessing metabolic flux in a glioma patient using ^{13}C MRS, lactate production was observed to be higher in the tumor tissue as compared to surrounding normal tissue from the occipital cortex [16]. Furthermore, in another study in six patients with chronic hepatic encephalopathy, cerebral Gln concentration was found to be increased while Glu levels decreased [14]. In a study measuring cerebral metabolism

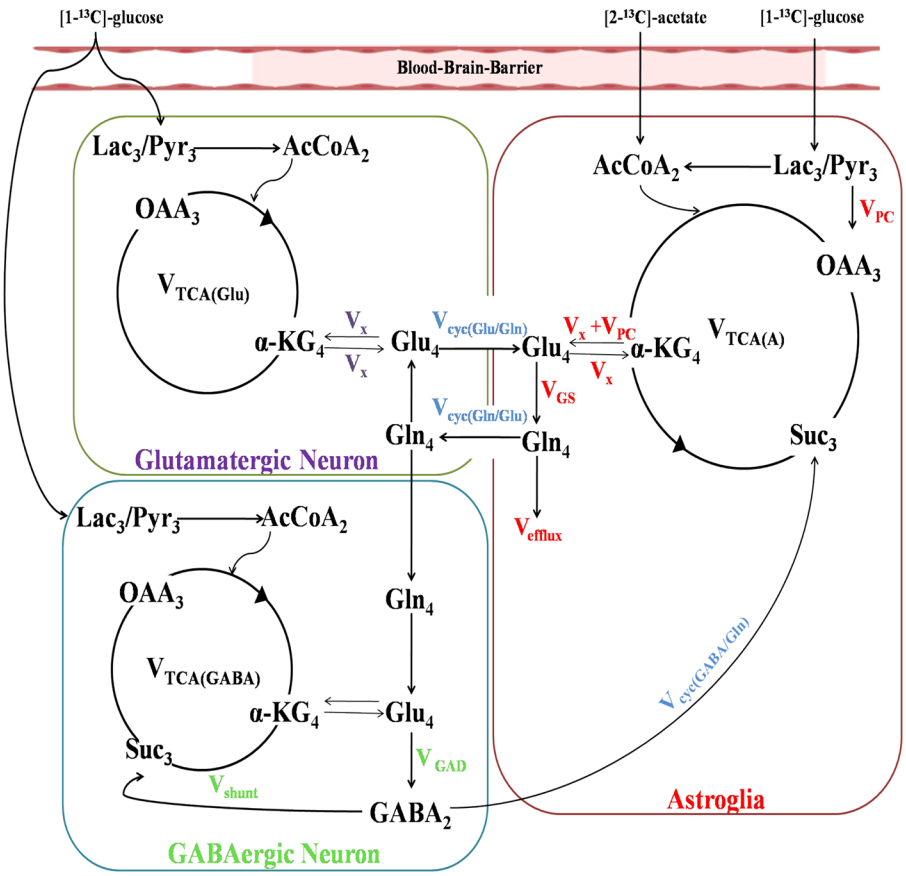

Fig. 9 A three-compartment model depicting important enzymatic fluxes and metabolic compartmentation in cerebral metabolism

in five patients with epilepsy, spectra were acquired from the occipital lobe of patients and changes in levels of glutamine synthesis were observed [74]. Ornithine transcarbamylase (OTC) is an enzyme that plays a major role in ammonia clearance from the blood. Its deficiency leads to toxic levels of ammonia accumulation. The cerebral glutamate turnover was assessed in six patients with partial OTC deficiency. The glutamate turnover was seen to be significantly reduced in such patients [75]. Many similar studies have been conducted in other neurological diseases like Alzheimer's disease, bipolar disorder, and depression which are described in the following section. In recent years, hyperpolarized ^{13}C MRS is used frequently to investigate tumor progression and metabolism in cancer patients [76].

Applications of ^{3}C MRS

^{13}C MRS (natural abundance or after ^{13}C labelled infusion) is used for noninvasive evaluation of brain metabolism [77]. Altered brain metabolism is implicated in several neurological diseases, such as in CHE [14], brain tumors [16], AD [15], and MDD [21]. Studies conducted using ^{1}H MRS have reported altered concentrations of GABA, Glu, NAA, and Gln in various psychiatric and neurological diseases, such as depression [78], epilepsy [79], liver cirrhosis [80], and neurodegenerative disorders [81]. However, measuring diverse metabolic pathways is absolutely vital as it can reveal fundamental changes occurring in the metabolic pathways and enzymes [20]. ^{13}C MRS has been identified as a powerful tool for detecting alterations in neuroenergetics for several classes of neurological and neuropsychiatric conditions (Fig. 10). An astonishing observation from in vivo ^{13}C MRS is that in case of orthotopic breast cancer, glycolysis serves as a potential metabolic marker of malignant transformation [82].

Bipolar Disorder and Schizophrenia

Bipolar disorder (BPD) causes excessive mood swings, and its progression can be attributed to genetic and environmental factors, including substance abuse and smoking [83–86]. Neuroenergetics and synaptic dysfunction have been implicated in BPD and SCZ, causing impaired neurodevelopment [84, 86]. Excessive Glu concentration in the synapse can lead to neuro-excitotoxicity [83, 87], which is a potential risk factor for the progression of BPD and SCZ. Patients with BPD have reported increased Glx levels [88], changes in NAA and phosphocreatine concentration, decrease in intercellular pH [89, 90], and elevated lactate signals localized to the caudate, anterior cingulate cortex, and frontal–subcortical [91]. ^{13}C MRS studies on BPD patients can help to observe discrete changes in Glu levels and neurotransmitter flux rates as well as to detect aberrant metabolism, which will likely open new avenues of therapeutic development.

Schizophrenia is a psychiatric disorder manifested by negative, positive, and/or cognitive symptoms [92]. Dopamine deficiency plays a critical role in aggravating negative symptoms and cognitive impairments in patients with SCZ [86]. Glu-mediated excitotoxicity is implicated in both preclinical models and clinical studies of SCZ [61]. One study reported an increase in Gln/Glu ratio during early onset of SCZ and decrease in the same during chronic stages [93]. Along with the unambiguous detection of Glu and Gln, ^{13}C MRS effectively distinguishes

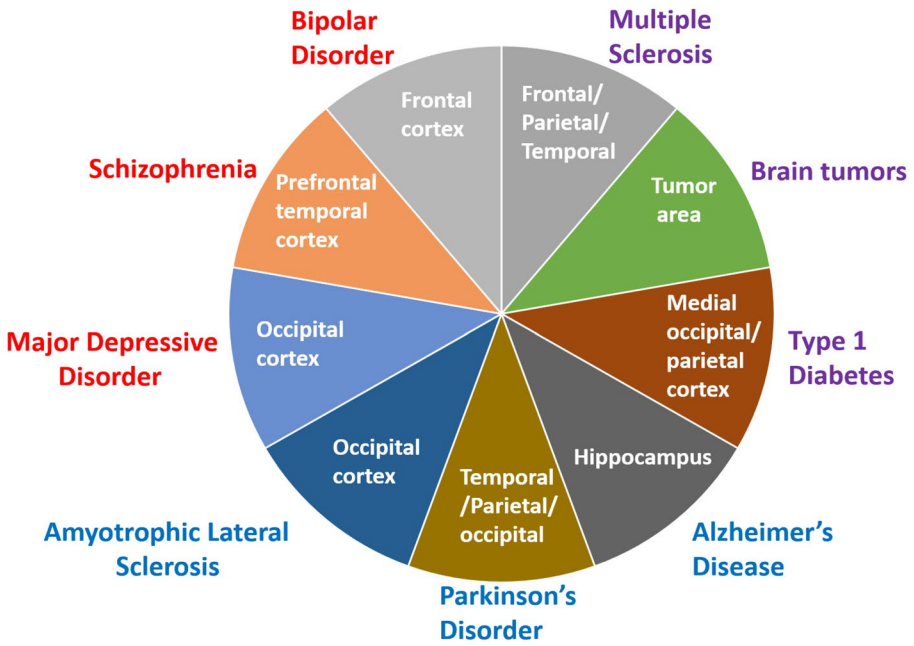

Fig. 10 Classification of different brain disorders, which are studied by ^{13}C MRS. Psychiatric, neurodegenerative, and general brain diseases are depicted. From existing literature, the brain region affected for the different diseases are also mentioned: Bipolar disorder [88]; Schizophrenia [137]; Major Depressive Disorder [21]; Amyotrophic Lateral Sclerosis [138]; Parkinson's disease [139]; Alzheimer's disease [139]; Type 1 diabetes [140]; Brain tumors [16]; Multiple sclerosis [141]

between intercellular and extracellular Glu pools [61]. This may help to develop treatment methods for patients with negative SCZ symptoms, including apathy, speech impairment, avolition [94–96], and several cognitive deficits [97].

Depression

Depression is a disabling mental disorder characterized by persistent negative thoughts about oneself along with the feeling of anhedonia (reduced pleasure in daily activities) [98, 99]. Neuroimaging techniques, including MRI, PET, and single-photon emission computerized tomography, are used to identify several neurological regions involved in the progression of MDD, especially the prefrontal cortex prone to impaired metabolism and atrophy of the amygdala, thalamus, and hippocampi [100].

In the pathogenesis of MDD, mitochondrial dysfunction in both glutamatergic and GABAergic neurons plays a critical role. Thus, ^{13}C MRS can be employed to detect alterations in neuroenergetics [21, 101, 102]. ^{1}H and ^{13}C spectra obtained from the occipital cortex, after the infusion of [1-^{13}C] glucose and $V_{TCA(n)}$ were relatively lower in the depression cohort compared to healthy controls. A significant reduction (≈ 26%) in the energy production of glutamatergic neurons was observed in the patients, although no difference was reported in the rates of Glu/Gln/GABA cycle fluxes.

Treatment for depression is targeted at the development of rapid-acting antidepressants [103]. Ketamine is a rapid-acting antidepressant with psychomimetic effect. Ketamine has been posited to have different mechanisms of action, the most prominent one being a competitive agonist of glutamatergic N-methyl-D-aspartate receptor [104]. It has also been theorized to act on the mTOR complex 1 pathway [105, 106]. mTOR is a protein kinase active in neurogenesis and circuit formation. Pre-clinical studies using rats have shown that the administration of sub-threshold dose of α-amino-3-hydroxy-5-methyl-4-isoxazole-propionic acid receptors (AMPAR) agonist Cx546 enhances the antidepressant effect of ketamine in forced-swim test. This indicates that ketamine potentially acts on AMPAR receptors and other downstream mechanisms to mitigate the symptoms of depression [107]. The mechanism of action of ketamine in the prefrontal cortex of healthy controls and depressed patients has been studied [108]. Ketamine administration exhibited an increase in the prefrontal cortex Glu/Gln cycle compared to those who were administered a placebo. Thus, developing novel drugs for redressing the biological causes of depression is vital to address the growing global burden of MDD [109].

Alzheimer's Disease

AD is a neurodegenerative disorder that affects memory and cognition [110]. Existing literature highlights various potential mechanisms of AD pathophysiology, including the cholinergic hypothesis [111], the amyloid hypothesis [112], the tau propagation hypothesis [113], the mitochondrial dysfunction, and the oxidative stress hypothesis [114]. Studies involving FDG–PET have demonstrated a reduction in resting-state brain glucose metabolism with an increase in the disease severity, especially in the primary cortical regions [115]. One study revealed that the ratio of enrichment Glu_2/Glu_4 between 60 and 100 min of infusion for patients with AD was 0.53 ± 0.11, whereas that for healthy controls was 0.76 ± 0.13, suggesting disruptive neuronal TCA cycle and reduced Glu neurotransmission [15]. After the infusion of [1-^{13}C]-glucose and [2-^{13}C]-acetate in young healthy adult controls and old healthy group, flux rates were calculated. $V_{TCA(n)}$ was observed to be 0.53 ± 0.03 µmol/g/min for the young adults as compared to 0.38 ± 0.04 µmol/g/min for the older subjects [116]. A decrease in NAA levels and the rate of GABA/Glu/Gln cycle by nearly 10% and 30%, respectively, were ultimately reported in the older subjects. However, the rate of astroglial TCA cycle was reported to be elevated [116]. As per MRI based findings of the occipital lobe, the rates were independent of age-related tissue loss. The increase in astroglial TCA cycle was attributed to neuronal impairment in the older subjects. Thus, it can be concluded that calculating the rate of glial TCA cycle after infusion of labeled acetate serves as a novel biomarker for prognostication of AD.

Brain Tumor

Brain tumors are attributed to the accumulation of mutations. [117]. Studies involving ^{1}H MRS have reportedly observed reduced NAA and increased Cho peaks in patients with brain tumors [118, 119]. This is in accordance with a study demonstrating the metabolism of brain tumor in situ using ^{13}C MRS [120]. Assessing lactate production kinetics is key to investigating the capacity of glucose metabolism in tumor progression and therapy feedback [16]. In this context, ^{13}C MRS is the only noninvasive in vivo method for lactate flux evaluation [121].

Chronic Hepatic Encephalopathy (CHE)

Studies involving ^{1}H MRS have revealed elevation and reduction in Gln and myo-inositol levels, respectively, in patients with CHE [122–124]. In studies involving ^{31}P MRS, a similar trend was reported along with the reduction in cerebral nucleoside triphosphate, phosphocreatine, and inorganic phosphate levels [125]. ^{13}C MRS-oriented studies

have revealed the role of Glu in CHE [14], wherein patients exhibited reduction in C2 Glu formation after being infused with [1-^{13}C]-labeled glucose. Along with this, reduced myo-inositol and elevated Gln levels were detected, which were also observed in ^{1}H MRS studies. Glu reduction was progressive with an increasing level of disease severity [Fig. 11(C)].

Hyperpolarized ^{13}C MRS

Hyperpolarized (HP) ^{13}C MRS is a relatively new method designed to increase the polarization of nuclear spin of ^{13}C to levels > 10^5 using low temperature, high magnetic field, and dynamic nuclear polarization (DNP) [126]. This technique has improved temporal resolution and rendered spatial resolution of 8-mL voxel volume, such that tissue metabolism can be imaged within clinically relevant timeframe [127]. DNP polarizes nuclear spins in the solid state, which is eventually dissolved in an appropriate solvent to obtain a liquid sample containing HP nuclear spins [126]. Moreover, effective polarization and subsequent signal enhancement in HP, ^{13}C MRS help eliminate the disadvantages associated with ^{1}H and conventional ^{13}C MRS (Fig. 12).

The longitudinal relaxation time (T1) is indicative of the time taken by magnetization to go back to the original position after application of the 180^{O} pulse. [1-^{13}C]-pyruvate is majorly used due to its longer T1 relaxation time of nearly 60 s in solution at 3 T [128]. Injection of HP [1-^{13}C]-pyruvate has proven beneficial to detect the metabolic flux of TCA cycle by following the labeling patterns of [1-^{13}C]-lactate (by lactate dehydrogenase), [1-^{13}C]-alanine (by alanine aminotransferase), and sometimes, [1-^{13}C]-bicarbonate (by pyruvate dehydrogenase) [129]. The entry of [1-^{13}C]-pyruvate is restricted by the blood–brain barrier (BBB) and makes it a rate-limiting factor. A lipophilic analogue [1-^{13}C]-ethyl-pyruvate reportedly enhances transport across the BBB, subsequently hydrolyzing into pyruvate [127]. Other studies have shown the efficacy of different tracers, such as [1-^{13}C]-lactate, [1-^{13}C]-Gln, and ketoisocaproic acid, to probe and interpret cancer-associated metabolic reprogramming [130–132]. In the very first study, the conversion of HP pyruvate to HP lactate was measured in patients with glioblastoma, wherein HP lactate production was noticeably

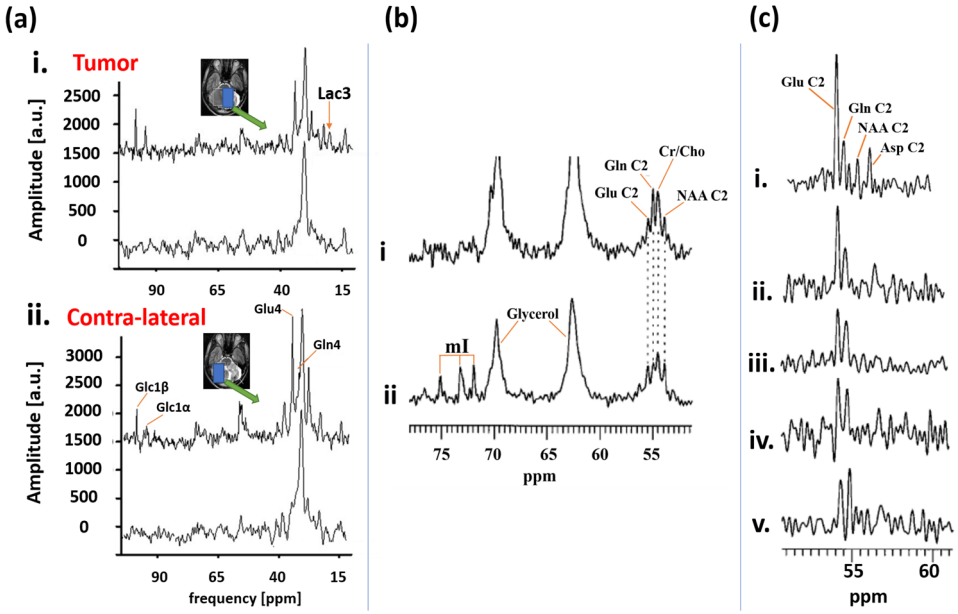

Fig. 11 Spectra from brain tumor and chronic hepatic encephalopathy in patients and controls **a** ^{13}C MR spectra of the tumor and contralateral voxel from a patient with malignant glioma showing baseline measurements (lower spectra) and last-hour measurements (upper spectra): (i) Spectra from the voxel placed at tumor indicating elevation in the lactate peak after [1-^{13}C]-glucose infusion. Resonance of this peak is absent in the voxel placed at normal tissue. (ii) Spectra from the contra-lateral voxel taken as control depicting several resonances of metabolic products of glucose. **b** Natural abundance ^{13}C spectra in CHE patient and control: (i) Natural abundance ^{13}C MRS of the most severe CHE patient showing altered peaks of various metabolites including Glu, Gln, and myo-inositol (mI). mI peak is completely depleted; Gln is splendidly increased; and Glu is slightly reduced. (ii) Natural abundance ^{13}C MRS of a control, where mI is easily identified along with other metabolites (Glu and Gln). **c** Spectra from one control and four CHE patients with increased disease severity as observed after the infusion of [1-^{13}C] glucose. (i) ^{13}C label accumulation in control indicating the different metabolite peaks, including Glu, Gln, Asp, and NAA. (ii–v) Spectra from four patients depicting continuous depletion of Glu C_2 labeling as the disease severity increases from patient B to patient E. NAA C_2 or aspartate C_2 is barely observed in CHE as they are noticed in the control. Glu: Glutamate; Gln: Glutamine; Asp: Aspartate; NAA: N-Acetyl aspartate. Image reproduced with permission from publisher [14, 16]

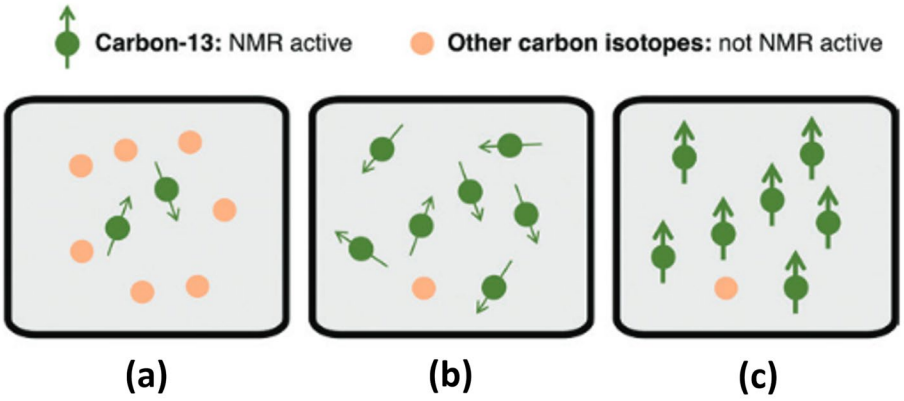

Fig. 12 Process of Hyperpolarization. **a** Distribution of a very small number of carbon atoms, which are ^{13}C-labeled at equilibrium with not well-aligned spins. Based on HP principle, high levels of polarization could be transferred to ^{13}C-labeled probes, which increases their MRI signal **b** ^{13}C enrichment results in the increased number of ^{13}C-labeled carbon atoms. Transfer of polarization takes place as the radicals are mixed with ^{13}C-labeled probes. **c** HP takes place in the mixture after it is placed in a polarizer at a magnetic field of 3.0–5.0 T and low temperature (nearly 1 K). This increases the number of aligned spins as illustrated above. Figure reproduced with permission from the publisher [128]

high [133]. Apart from the brain, HP ^{13}C MRS has been implemented in prostate and breast cancers [134, 135].

Conclusion and Future Prospects

MRS is a noninvasive diagnostic modality with potential immense applications in clinical studies. ^{1}H and ^{31}P MRS techniques are used to detect metabolites, such as choline, NAA, creatine, inorganic phosphate, phosphodiesters, and ATP-like energy metabolites. Moreover, cerebral pH and concentrations of different neurotransmitters, including Gln, Glu, and GABA, are detected in clinical settings [4]. ^{13}C MRS noninvasively measures both neuronal and glial metabolism as well as Glu and GABA neurotransmission. Apart from glucose, ^{13}C MRS has further delineated the role of other substrates, such as lactate, acetate, and ketone bodies, in cerebral neuroenergetics in healthy and diseased conditions. Although ^{13}C MRS has drawbacks of low sensitivity, decoupling-associated heat generation, and substantial technical costs, it has been gaining precedence due to its ability to track information regarding the etiology and pathophysiology of several psychiatric and neurodegenerative diseases.

With major technological advancements, such as B0 shimming, broadband decoupling–nuclear Overhauser effect (NOE), and HP ^{13}C MRS, ^{13}C MRS technology is rapidly evolving. It has potential therapeutic and clinical applications as it qualitatively surpasses other techniques, such as invasive FDG–PET. Additionally, unambiguous quantitation of neurometabolites and the rate of different metabolic fluxes in diseased conditions can be determining factors in the differential diagnosis of various neurological diseases. Research on pulse sequences, dual-tuned coils, contrast agents, test–retest, reliability, and feasibility experiments can all contribute to the development of in vivo ^{13}C MRS in human research. In addition, the coil design and signal acquisition methods need to be thoroughly examined for their application in various brain environments to identify the etiology and direct cause of diseases. We propose that in the future, X nuclei (^{23}Na, ^{33}S, ^{35}Cl, ^{39} K, ^{17}O, ^{25} Mg, ^{27}Al, and ^{67}Zn) be investigated for the purpose of discovering biomarkers for early diagnosis and treatment of many neurological disorders. This is a focused area of research in our laboratory where ^{13}C MRS techniques will be employed to identify biomarkers for Alzheimer's disease and neuropsychiatric disorders.

Acknowledgements Professor Pravat K. Mandal (Principal Investigator) thanks for partial financial support from various agencies: Tata Innovation Fellow (Department of Biotechnology, Ministry of Science and Technology, Government of India) (Award No. BT/HRD/01/05/2015 to PKM), Indo Australian grant strategic funding to PKM, (Grant No. BT/Indo-Aus/10/31/2016 to PKM), and the ministry of information technology (Grant No. 4(5)/201-ITEA to PKM). Additionally, we would also like to extend our gratitude to the reviewers whose valuable suggestions enabled us to improve and enrich the manuscript to the greatest degree.

Author Contributions Prof. PKM (Principal Investigator) was involved in idea conceptualization, literature review, data review, and writing and editing the manuscript. Ms. As and Ms. RGR were involved in literature search, figure preparation, and writing the manuscript. Dr. JM and Dr YA were involved in discussion and writing the manuscript.

Funding Prof. Pravat K. Mandal (Principal Investigator) thanks for partial financial support from various agencies: Tata Innovation

Fellowship (Department of Biotechnology, Ministry of Science and Technology, Government of India) (Award No. BT/HRD/01/05/2015), Indo Australian grant strategic funding to PKM, (Grant No. BT/Indo-Aus/10/31/2016), and the Ministry of Information Technology (Grant No. 4(5)/201-ITEA).

Declarations

Conflict of interest There are no conflicts of interest.

Data Availability Not Applicable.

Code Availability Not Applicable.

References

1. Tognarelli JM, Dawood M, Shariff MI, Grover VP, Crossey MM, Cox IJ, Taylor-Robinson SD, McPhail MJ (2015) Magnetic resonance spectroscopy: principles and techniques: lessons for clinicians. J Clin Exp Hepatol 5:320–328
2. Gujar SK, Maheshwari S, Bjorkman-Burtscher I, Sundgren PC (2005) Magnetic resonance spectroscopy. J Neuroophthalmol 25:217–226
3. Cady EB, Costello AM, Dawson MJ, Delpy DT, Hope PL, Reynolds EO, Tofts PS, Wilkie DR (1983) Non-invasive investigation of cerebral metabolism in newborn infants by phosphorus nuclear magnetic resonance spectroscopy. Lancet 1:1059–1062
4. Duncan JS (1996) Magnetic resonance spectroscopy. Epilepsia 37:598–605
5. Ross B, Lin A, Harris K, Bhattacharya P, Schweinsburg B (2003) Clinical experience with 13C MRS in vivo. NMR Biomed 16:358–369
6. Kurhanewicz J, Bok R, Nelson SJ, Vigneron DB (2008) Current and potential applications of clinical 13C MR spectroscopy. J Nucl Med 49:341–344
7. Morris P, Bachelard H (2003) Reflections on the application of 13C-MRS to research on brain metabolism. NMR Biomed 16:303–312
8. Phelps ME, Huang SC, Hoffman EJ, Selin C, Sokoloff L, Kuhl DE (1979) Tomographic measurement of local cerebral glucose metabolic rate in humans with (F-18)2-fluoro-2-deoxy-D-glucose: validation of method. Ann Neurol 6:371–388
9. Reivich M, Kuhl D, Wolf A, Greenberg J, Phelps M, Ido T, Casella V, Fowler J, Hoffman E, Alavi A, Som P, Sokoloff L (1979) The [18F]fluorodeoxyglucose method for the measurement of local cerebral glucose utilization in man. Circ Res 44:127–137
10. Sokoloff L, Reivich M, Kennedy C, Des Rosiers MH, Patlak CS, Pettigrew KD, Sakurada O, Shinohara M (1977) The [14C]deoxyglucose method for the measurement of local cerebral glucose utilization: theory, procedure, and normal values in the conscious and anesthetized albino rat. J Neurochem 28:897–916
11. Raichle ME, Larson KB, Phelps ME, Grubb RL Jr, welch MJ, Ter-Pogossian MM, (1975) In vivo measurement of brain glucose transport and metabolism employing glucose- -11C. Am J Physiol 228:1936–1948
12. Faghihi R, Zeinali-Rafsanjani B, Mosleh-Shirazi MA, Saeedi-Moghadam M, Lotfi M, Jalli R, Iravani V (2017) Magnetic resonance spectroscopy and its clinical applications: a review. J Med Imaging Radiat Sci 48:233–253
13. Weiner MW, Hetherington HP (1989) The power of the proton. Radiology 172:318–320
14. Bluml S, Moreno-Torres A, Ross BD (2001) [1-13C]glucose MRS in chronic hepatic encephalopathy in man. Magn Reson Med 45:981–993
15. Lin AP, Shic F, Enriquez C, Ross BD (2003) Reduced glutamate neurotransmission in patients with Alzheimer's disease – an in vivo (13)C magnetic resonance spectroscopy study. MAGMA 16:29–42
16. Wijnen JP, Van der Graaf M, Scheenen TW, Klomp DW, de Galan BE, Idema AJ, Heerschap A (2010) In vivo 13C magnetic resonance spectroscopy of a human brain tumor after application of 13C-1-enriched glucose. Magn Reson Imaging 28:690–697
17. Rodrigues TB, Cerdan S (2005) 13C MRS: an outstanding tool for metabolic studies. Concepts Magnet. Resonance 27A(1):1–16
18. Li N, Li S, Shen J (2017) High field in vivo (13)C magnetic resonance spectroscopy of brain by random radiofrequency heteronuclear decoupling and data undersampling. Front Phys 5
19. van Zijl PC, Rothman D (1995) NMR studies of brain 13C-glucose uptake and metabolism: present status. Magn Reson Imaging 13:1213–1221
20. Rothman DL, de Graaf RA, Hyder F, Mason GF, Behar KL, De Feyter HM (2019) In vivo (13) C and (1) H-[(13) C] MRS studies of neuroenergetics and neurotransmitter cycling, applications to neurological and psychiatric disease and brain cancer. NMR Biomed 32:e4172
21. Abdallah CG, Jiang L, De Feyter HM, Fasula M, Krystal JH, Rothman DL, Mason GF, Sanacora G (2014) Glutamate metabolism in major depressive disorder. Am J Psychiatry 171:1320–1327
22. Beckmann N, Muller S (1991) Natural-abundance 13C spectroscopic imaging applied to humans. J Magn Reson 93:186–194
23. Avison MJ, Rothman DL, Nadel E, Shulman RG (1988) Detection of human muscle glycogen by natural abundance 13C NMR. Proc Natl Acad Sci USA 85:1634–1636
24. Rothman DL, De Feyter HM, de Graaf RA, Mason GF, Behar KL (2011) 13C MRS studies of neuroenergetics and neurotransmitter cycling in humans. NMR Biomed 24:943–957
25. Beckmann N, Turkalj I, Seelig J, Keller U (1991) 13C NMR for the assessment of human brain glucose metabolism in vivo. Biochemistry 30:6362–6366
26. Ordidce RJ, ConnellyB. LJA, A (1986) Image-selected in viva spectroscopy (ISIS). A New Technique for Spatially Selective NMR Spectroscopy J Magn Reson 66:283–294
27. Gruetter R, Novotny EJ, Boulware SD, Rothman DL, Mason GF, Shulman GI, Shulman RG, Tamborlane WV (1992) Direct measurement of brain glucose concentrations in humans by 13C NMR spectroscopy. Proc Natl Acad Sci USA 89:1109–1112
28. Shaka. AJ, Reeler. J, Freeman R (1983) An improved sequence for broadband decoupling: WALTZ-16. J Magn Reson 52:335–338
29. Gruetter R, Adriany G, Merkle H, Andersen PM (1996) Broadband decoupled, 1H-localized 13C MRS of the human brain at 4 Tesla. Magn Reson Med 36:659–664
30. Gruetter R, Seaquist ER, Kim S, Ugurbil K (1998) Localized in vivo 13C-NMR of glutamate metabolism in the human brain: initial results at 4 tesla. Dev Neurosci 20:380–388
31. Watanabe H, Umeda M, Ishihara Y, Okamoto K, Oshio K, Kanamatsu T, Tsukada Y (2000) Human brain glucose metabolism mapping using multislice 2D (1)H-(13)C correlation HSQC spectroscopy. Magn Reson Med 43:525–533
32. Klomp DW, Renema WK, van der Graaf M, de Galan BE, Kentgens AP, Heerschap A (2006) Sensitivity-enhanced 13C MR spectroscopy of the human brain at 3 Tesla. Magn Reson Med 55:271–278
33. Li S, An L, Yu S, Ferraris Araneta M, Johnson CS, Wang S, Shen J (2016) (13)C MRS of human brain at 7 Tesla using [2-(13)

C]glucose infusion and low power broadband stochastic proton decoupling. Magn Reson Med 75:954–961
34. Sanchez-Heredia JD, Olin RB, McLean MA, Laustsen C, Hansen AE, Hanson LG, Ardenkjaer-Larsen JH (2020) Multi-site benchmarking of clinical (13)C RF coils at 3T. J Magn Reson 318:106798
35. Mandal PK, Shukla D (2020) KALPANA: advanced spectroscopic signal processing platform for improved accuracy to aid in early diagnosis of brain disorders in clinical setting. J Alzheimers Dis 75:397–402
36. Goluch S, Frass-Kriegl R, Meyerspeer M, Pichler M, Sieg J, Gajdošík M, Krššák M, Laistler E (2018) Proton-decoupled carbon magnetic resonance spectroscopy in human calf muscles at 7 T using a multi-channel radiofrequency coil. Sci Rep 8:6211
37. Camandola S, Mattson MP (2017) Brain metabolism in health, aging, and neurodegeneration. EMBO J 36:1474–1492
38. Carluccio G, Collins CM (2019) Optimization of the order and spacing of sequences in an MRI exam to reduce the maximum temperature and thermal dose. Magn Reson Med 81:2161–2166
39. Allison J, Yanasak N (2015) What MRI sequences produce the highest specific absorption rate (SAR), and is there something we should be doing to reduce the SAR during standard examinations? AJR Am J Roentgenol 205:W140
40. Valette J, Tiret B, Boumezbeur F (2017) Experimental strategies for in vivo(13)C NMR spectroscopy. Anal Biochem 529:216–228
41. Kreis R (2004) Issues of spectral quality in clinical 1H-magnetic resonance spectroscopy and a gallery of artifacts. NMR Biomed 17:361–381
42. Kumaragamage C, De Feyter HM, Brown P, McIntyre S, Nixon TW, de Graaf RA (2020) Robust outer volume suppression utilizing elliptical pulsed second order fields (ECLIPSE) for human brain proton MRSI. Magn Reson Med 83:1539–1552
43. Boer VO, van de Lindt T, Luijten PR, Klomp DW (2015) Lipid suppression for brain MRI and MRSI by means of a dedicated crusher coil. Magn Reson Med 73:2062–2068
44. Sonnay S, Gruetter R, Duarte JMN (2017) How energy metabolism supports cerebral function: insights from (13)C magnetic resonance studies in vivo. Front Neurosci 11:288
45. de Graaf RA, Mason GF, Patel AB, Behar KL, Rothman DL (2003) In vivo 1H-[13C]-NMR spectroscopy of cerebral metabolism. NMR Biomed 16:339–357
46. de Graaf RA, Rothman DL, Behar KL (2011) State of the art direct 13C and indirect 1H-[13C] NMR spectroscopy in vivo A practical guide. NMR Biomed 24:958–972
47. Rodrigues TB, Valette J, Bouzier-Sore AK (2013) (13)C NMR spectroscopy applications to brain energy metabolism. Front Neuroenergetics 5:9
48. Mason GF, Rothman DL, Behar KL, Shulman RG (1992) NMR determination of the TCA cycle rate and alpha-ketoglutarate/glutamate exchange rate in rat brain. J Cereb Blood Flow Metab 12:434–447
49. Badar-Goffer RS, Bachelard HS, Morris PG (1990) Cerebral metabolism of acetate and glucose studied by 13C-n.m.r. spectroscopy. A technique for investigating metabolic compartmentation in the brain. Biochem J 266:133–139
50. Cerdan S, Kunnecke B, Seelig J (1990) Cerebral metabolism of [1,2–13C2]acetate as detected by in vivo and in vitro 13C NMR. J Biol Chem 265:12916–12926
51. Deelchand DK, Nelson C, Shestov AA, Ugurbil K, Henry PG (2009) Simultaneous measurement of neuronal and glial metabolism in rat brain in vivo using co-infusion of [1,6–13C2]glucose and [1,2–13C2]acetate. J Magn Reson 196:157–163
52. Kunnecke B, Cerdan S, Seelig J (1993) Cerebral metabolism of [1,2–13C2]glucose and [U-13C4]3-hydroxybutyrate in rat brain as detected by 13C NMR spectroscopy. NMR Biomed 6:264–277
53. Wyss MT, Jolivet R, Buck A, Magistretti PJ, Weber B (2011) In vivo evidence for lactate as a neuronal energy source. J Neurosci 31:7477–7485
54. Pan JW, Mason GF, Vaughan JT, Chu WJ, Zhang Y, Hetherington HP (1997) 13C editing of glutamate in human brain using J-refocused coherence transfer spectroscopy at 4.1 T. Magn Reson Med 37:355–358
55. Webb GA (2008) Modern magnetic resonance. Springer, London
56. Mason GF, Falk Petersen K, de Graaf RA, Kanamatsu T, Otsuki T, Shulman GI, Rothman DL (2003) A comparison of (13)C NMR measurements of the rates of glutamine synthesis and the tricarboxylic acid cycle during oral and intravenous administration of [1-(13)C]glucose. Brain Res Protoc 10:181–190
57. Hyder F, Patel AB, Gjedde A, Rothman DL, Behar KL, Shulman RG (2006) Neuronal-glial glucose oxidation and glutamatergic-GABAergic function. J Cereb Blood Flow Metab 26:865–877
58. Zhou Y, Danbolt NC (2014) Glutamate as a neurotransmitter in the healthy brain. J Neural Transm (Vienna) 121:799–817
59. Sibson NR, Dhankhar A, Mason GF, Behar KL, Rothman DL, Shulman RG (1997) In vivo 13C NMR measurements of cerebral glutamine synthesis as evidence for glutamate-glutamine cycling. Proc Natl Acad Sci USA 94:2699–2704
60. Sibson NR, Dhankhar A, Mason GF, Rothman DL, Behar KL, Shulman RG (1998) Stoichiometric coupling of brain glucose metabolism and glutamatergic neuronal activity. Proc Natl Acad Sci USA 95:316–321
61. Plitman E, Nakajima S, de la Fuente-Sandoval C, Gerretsen P, Chakravarty MM, Kobylianskii J, Chung JK, Caravaggio F, Iwata Y, Remington G, Graff-Guerrero A (2014) Glutamate-mediated excitotoxicity in schizophrenia: a review. Eur Neuropsychopharmacol 24:1591–1605
62. Patel AB, de Graaf RA, Mason GF, Rothman DL, Shulman RG, Behar KL (2005) The contribution of GABA to glutamate/glutamine cycling and energy metabolism in the rat cortex in vivo. Proc Natl Acad Sci USA 102:5588–5593
63. Bahadur Patel A, Veeraiah P, Shameem M, Mahesh Kumar J, Saba K (2021) Impaired GABAergic and glutamatergic neurometabolic activity in aged mice brain as measured by (1) H-[(13)C]-NMR spectroscopy. FASEB J 35:e21321
64. Lanz B, Gruetter R, Duarte JM (2013) Metabolic flux and compartmentation analysis in the brain in vivo. Front Endocrinol (Lausanne) 4:156
65. Henry PG, Adriany G, Deelchand D, Gruetter R, Marjanska M, Oz G, Seaquist ER, Shestov A, Ugurbil K (2006) In vivo 13C NMR spectroscopy and metabolic modeling in the brain: a practical perspective. Magn Reson Imaging 24:527–539
66. Berl S, Lajtha A, Waelsch H (1961) Amino acid and protein metabolism-VI cerebral compartments of glutamic acid metabolism. J Neurochem 7:186–197
67. Cruz F, Cerdan S (1999) Quantitative 13C NMR studies of metabolic compartmentation in the adult mammalian brain. NMR Biomed 12:451–462
68. Hertz L (2004) Intercellular metabolic compartmentation in the brain: past, present and future. Neurochem Int 45:285–296
69. Bluml S, Moreno-Torres A, Shic F, Nguy CH, Ross BD (2002) Tricarboxylic acid cycle of glia in the in vivo human brain. NMR Biomed 15:1–5
70. Badar-Goffer RS, Ben-Yoseph O, Bachelard HS, Morris PG (1992) Neuronal-glial metabolism under depolarizing conditions. A 13C-n.m.r. study. Biochem J 282 (Pt 1):225–230
71. Duarte JM, Lanz B, Gruetter R (2011) Compartmentalized Cerebral Metabolism of [1,6-(13)C]Glucose Determined by in vivo (13)C NMR Spectroscopy at 14.1 T. Front Neuroenerget 3:3
72. Lai M, Lanz B, Poitry-Yamate C, Romero JF, Berset CM, Cudalbu C, Gruetter R (2018) In vivo (13)C MRS in the mouse brain at 14.1 Tesla and metabolic flux quantification under

infusion of [1,6-(13)C2]glucose. J Cereb Blood Flow Metab 38:1701–1714
73. Duarte JM, Gruetter R (2013) Glutamatergic and GABAergic energy metabolism measured in the rat brain by (13) C NMR spectroscopy at 14.1 T. J Neurochem 126:579–590
74. Otsuki T, Nakama H, Kanamatsu T, Tsukada Y (2005) Glutamate metabolism in epilepsy: 13C-magnetic resonance spectroscopy observation in the human brain. NeuroReport 16:2057–2060
75. Gropman AL, Sailasuta N, Harris KC, Abulseoud O, Ross BD (2009) Ornithine transcarbamylase deficiency with persistent abnormality in cerebral glutamate metabolism in adults. Radiology 252:833–841
76. Najac C, Ronen SM (2016) MR molecular imaging of brain cancer metabolism using hyperpolarized 13C magnetic resonance spectroscopy. Top Magn Reson Imaging 25:187–196
77. Bluml S, Hwang JH, Moreno A, Ross BD (2000) Novel peak assignments of in vivo (13)C MRS in human brain at 1.5 T. J Magn Reson 143:292–298
78. Gruber S, Frey R, Mlynarik V, Stadlbauer A, Heiden A, Kasper S, Kemp GJ, Moser E (2003) Quantification of metabolic differences in the frontal brain of depressive patients and controls obtained by 1H-MRS at 3 Tesla. Invest Radiol 38:403–408
79. Novotny EJ Jr, Hyder F, Shevell M, Rothman DL (1999) GABA changes with vigabatrin in the developing human brain. Epilepsia 40:462–466
80. Lee JH, Seo DW, Lee YS, Kim ST, Mun CW, Lim TH, Min YI, Suh DJ (1999) Proton magnetic resonance spectroscopy (1H-MRS) findings for the brain in patients with liver cirrhosis reflect the hepatic functional reserve. Am J Gastroenterol 94:2206–2213
81. Martin WR (2007) MR spectroscopy in neurodegenerative disease. Mol Imaging Biol 9:196–203
82. Rivenzon-Segal D, Margalit R, Degani H (2002) Glycolysis as a metabolic marker in orthotopic breast cancer, monitored by in vivo (13)C MRS. Am J Physiol Endocrinol Metab 283:E623-630
83. Mark LP, Prost RW, Ulmer JL, Smith MM, Daniels DL, Strottmann JM, Brown WD, Hacein-Bey L (2001) Pictorial review of glutamate excitotoxicity: fundamental concepts for neuroimaging. AJNR Am J Neuroradiol 22:1813–1824
84. Kato T (2007) Mitochondrial dysfunction as the molecular basis of bipolar disorder: therapeutic implications. CNS Drugs 21:1–11
85. Burmeister M, McInnis MG, Zollner S (2008) Psychiatric genetics: progress amid controversy. Nat Rev Genet 9:527–540
86. Duarte JMN, Xin L (2019) Magnetic resonance spectroscopy in schizophrenia: evidence for glutamatergic dysfunction and impaired energy metabolism. Neurochem Res 44:102–116
87. Dong XX, Wang Y, Qin ZH (2009) Molecular mechanisms of excitotoxicity and their relevance to pathogenesis of neurodegenerative diseases. Acta Pharmacol Sin 30:379–387
88. Gigante AD, Bond DJ, Lafer B, Lam RW, Young LT, Yatham LN (2012) Brain glutamate levels measured by magnetic resonance spectroscopy in patients with bipolar disorder: a meta-analysis. Bipolar Disord 14:478–487
89. Hamakawa H, Murashita J, Yamada N, Inubushi T, Kato N, Kato T (2004) Reduced intracellular pH in the basal ganglia and whole brain measured by 31P-MRS in bipolar disorder. Psychiatry Clin Neurosci 58:82–88
90. Yildiz-Yesiloglu A, Ankerst DP (2006) Neurochemical alterations of the brain in bipolar disorder and their implications for pathophysiology: a systematic review of the in vivo proton magnetic resonance spectroscopy findings. Prog Neuropsychopharmacol Biol Psychiatry 30:969–995
91. Chu WJ, Delbello MP, Jarvis KB, Norris MM, Kim MJ, Weber W, Lee JH, Strakowski SM, Adler CM (2013) Magnetic resonance spectroscopy imaging of lactate in patients with bipolar disorder. Psychiatry Res 213:230–234
92. Kay SR, Sevy S (1990) Pyramidical model of schizophrenia. Schizophr Bull 16:537–545
93. Madeira C, Alheira FV, Calcia MA, Silva TCS, Tannos FM, Vargas-Lopes C, Fisher M, Goldenstein N, Brasil MA, Vinogradov S, Ferreira ST, Panizzutti R (2018) Blood levels of glutamate and glutamine in recent onset and chronic schizophrenia. Front Psychiatry 9:713
94. Kirkpatrick B, Fenton WS, Carpenter WT Jr, Marder SR (2006) The NIMH-MATRICS consensus statement on negative symptoms. Schizophr Bull 32:214–219
95. (2014) Diagnostic and Statistical Manual of Mental Disorders: DSM-5 (5th edition). Reference Reviews 28:36–37
96. Mitra S, Mahintamani T, Kavoor AR, Nizamie SH (2016) Negative symptoms in schizophrenia. Ind Psychiatry J 25:135–144
97. Bowie CR, Harvey PD (2006) Cognitive deficits and functional outcome in schizophrenia. Neuropsychiatr Dis Treat 2:531–536
98. Health NIoM (2018) Depression.
99. Organisation WH (2020) Depression.
100. Pandya M, Altinay M, Malone DA Jr, Anand A (2012) Where in the brain is depression? Curr Psychiatry Rep 14:634–642
101. Luscher B, Shen Q, Sahir N (2011) The GABAergic deficit hypothesis of major depressive disorder. Mol Psychiatry 16:383–406
102. Manji H, Kato T, Di Prospero NA, Ness S, Beal MF, Krams M, Chen G (2012) Impaired mitochondrial function in psychiatric disorders. Nat Rev Neurosci 13:293–307
103. Gerhard DM, Duman RS (2018) Rapid-acting antidepressants: mechanistic insights and future directions. Curr Behav Neurosci Rep 5:36–47
104. Krystal JH, Karper LP, Seibyl JP, Freeman GK, Delaney R, Bremner JD, Heninger GR, Bowers MB Jr, Charney DS (1994) Subanesthetic effects of the noncompetitive NMDA antagonist, ketamine, in humans. Psychotomimetic, perceptual, cognitive, and neuroendocrine responses. Arch Gen Psychiatry 51:199–214
105. Zanos P, Gould TD (2018) Mechanisms of ketamine action as an antidepressant. Mol Psychiatry 23:801–811
106. Matveychuk D, Thomas RK, Swainson J, Khullar A, MacKay MA, Baker GB, Dursun SM (2020) Ketamine as an antidepressant: overview of its mechanisms of action and potential predictive biomarkers. Ther Adv Psychopharmacol 10:2045125320916657
107. Zhou W, Wang N, Yang C, Li XM, Zhou ZQ, Yang JJ (2014) Ketamine-induced antidepressant effects are associated with AMPA receptors-mediated upregulation of mTOR and BDNF in rat hippocampus and prefrontal cortex. Eur Psychiatry 29:419–423
108. Abdallah CG, De Feyter HM, Averill LA, Jiang L, Averill CL, Chowdhury GMI, Purohit P, de Graaf RA, Esterlis I, Juchem C, Pittman BP, Krystal JH, Rothman DL, Sanacora G, Mason GF (2018) The effects of ketamine on prefrontal glutamate neurotransmission in healthy and depressed subjects. Neuropsychopharmacology 43:2154–2160
109. Malgorzata P, Pawel K, Iwona ML, Brzostek T, Andrzej P (2020) Glutamatergic dysregulation in mood disorders: opportunities for the discovery of novel drug targets. Expert Opin Ther Targets 24:1187–1209
110. Liu PP, Xie Y, Meng XY, Kang JS (2019) History and progress of hypotheses and clinical trials for Alzheimer's disease. Signal Transduct Target Ther 4:29
111. Terry AV Jr, Buccafusco JJ (2003) The cholinergic hypothesis of age and Alzheimer's disease-related cognitive deficits: recent challenges and their implications for novel drug development. J Pharmacol Exp Ther 306:821–827

112. Hardy J, Selkoe DJ (2002) The amyloid hypothesis of Alzheimer's disease: progress and problems on the road to therapeutics. Science 297:353–356
113. Lewis J, Dickson DW (2016) Propagation of tau pathology: hypotheses, discoveries, and yet unresolved questions from experimental and human brain studies. Acta Neuropathol 131:27–48
114. Lin MT, Beal MF (2006) Mitochondrial dysfunction and oxidative stress in neurodegenerative diseases. Nature 443:787–795
115. Rapoport SI (1999) Functional brain imaging in the resting state and during activation in Alzheimer's disease. Implications for disease mechanisms involving oxidative phosphorylation. Ann N Y Acad Sci 893:138–153
116. Boumezbeur F, Mason GF, de Graaf RA, Behar KL, Cline GW, Shulman GI, Rothman DL, Petersen KF (2010) Altered brain mitochondrial metabolism in healthy aging as assessed by in vivo magnetic resonance spectroscopy. J Cereb Blood Flow Metab 30:211–221
117. DeAngelis LM (2001) Brain tumors. N Engl J Med 344:114–123
118. Sjobakk TE, Lundgren S, Kristoffersen A, Singstad T, Svarliaunet AJ, Sonnewald U, Gribbestad IS (2006) Clinical 1H magnetic resonance spectroscopy of brain metastases at 1.5T and 3T. Acta Radiol 47:501–508
119. Calvar JA, Meli FJ, Romero C, Calcagno ML, Yanez P, Martinez AR, Lambre H, Taratuto AL, Sevlever G (2005) Characterization of brain tumors by MRS, DWI and Ki-67 labeling index. J Neurooncol 72:273–280
120. Maher EA, Marin-Valencia I, Bachoo RM, Mashimo T, Raisanen J, Hatanpaa KJ, Jindal A, Jeffrey FM, Choi C, Madden C, Mathews D, Pascual JM, Mickey BE, Malloy CR, DeBerardinis RJ (2012) Metabolism of [U-13 C]glucose in human brain tumors in vivo. NMR Biomed 25:1234–1244
121. Brender JR, Kishimoto S, Merkle H, Reed G, Hurd RE, Chen AP, Ardenkjaer-Larsen JH, Munasinghe J, Saito K, Seki T, Oshima N, Yamamoto K, Choyke PL, Mitchell J, Krishna MC (2019) Dynamic imaging of glucose and lactate metabolism by (13) C-MRS without hyperpolarization. Sci Rep 9:3410
122. Kreis R, Ross BD, Farrow NA, Ackerman Z (1992) Metabolic disorders of the brain in chronic hepatic encephalopathy detected with H-1 MR spectroscopy. Radiology 182:19–27
123. Haussinger D, Laubenberger J, vom Dahl S, Ernst T, Bayer S, Langer M, Gerok W, Hennig J (1994) Proton magnetic resonance spectroscopy studies on human brain myo-inositol in hypo-osmolarity and hepatic encephalopathy. Gastroenterology 107:1475–1480
124. Ross BD, Jacobson S, Villamil F, Korula J, Kreis R, Ernst T, Shonk T, Moats RA (1994) Subclinical hepatic encephalopathy: proton MR spectroscopic abnormalities. Radiology 193:457–463
125. Bluml S, Zuckerman E, Tan J, Ross BD (1998) Proton-decoupled 31P magnetic resonance spectroscopy reveals osmotic and metabolic disturbances in human hepatic encephalopathy. J Neurochem 71:1564–1576
126. Ardenkjaer-Larsen JH, Fridlund B, Gram A, Hansson G, Hansson L, Lerche MH, Servin R, Thaning M, Golman K (2003) Increase in signal-to-noise ratio of > 10,000 times in liquid-state NMR. Proc Natl Acad Sci USA 100:10158–10163
127. Grist JT, Miller JJ, Zaccagna F, McLean MA, Riemer F, Matys T, Tyler DJ, Laustsen C, Coles AJ, Gallagher FA (2020) Hyperpolarized (13)C MRI: a novel approach for probing cerebral metabolism in health and neurological disease. J Cereb Blood Flow Metab 40:1137–1147
128. Wang ZJ, Ohliger MA, Larson PEZ, Gordon JW, Bok RA, Slater J, Villanueva-Meyer JE, Hess CP, Kurhanewicz J, Vigneron DB (2019) Hyperpolarized (13)C MRI: state of the art and future directions. Radiology 291:273–284
129. Le Page LM, Guglielmetti C, Taglang C, Chaumeil MM (2020) Imaging brain metabolism using hyperpolarized (13)c magnetic resonance spectroscopy. Trends Neurosci 43:343–354
130. Josan S, Hurd R, Billingsley K, Senadheera L, Park JM, Yen YF, Pfefferbaum A, Spielman D, Mayer D (2013) Effects of isoflurane anesthesia on hyperpolarized (13)C metabolic measurements in rat brain. Magn Reson Med 70:1117–1124
131. Chaumeil MM, Larson PE, Woods SM, Cai L, Eriksson P, Robinson AE, Lupo JM, Vigneron DB, Nelson SJ, Pieper RO, Phillips JJ, Ronen SM (2014) Hyperpolarized [1-13C] glutamate: a metabolic imaging biomarker of IDH1 mutational status in glioma. Cancer Res 74:4247–4257
132. Takado Y, Cheng T, Bastiaansen JAM, Yoshihara HAI, Lanz B, Mishkovsky M, Lengacher S, Comment A (2018) Hyperpolarized (13)C magnetic resonance spectroscopy reveals the rate-limiting role of the blood-brain barrier in the cerebral uptake and metabolism of l-lactate in vivo. ACS Chem Neurosci 9:2554–2562
133. Miloushev VZ, Granlund KL, Boltyanskiy R, Lyashchenko SK, DeAngelis LM, Mellinghoff IK, Brennan CW, Tabar V, Yang TJ, Holodny AI, Sosa RE, Guo YW, Chen AP, Tropp J, Robb F, Keshari KR (2018) Metabolic imaging of the human brain with hyperpolarized (13)C pyruvate demonstrates (13)C lactate production in brain tumor patients. Cancer Res 78:3755–3760
134. Nelson SJ, Kurhanewicz J, Vigneron DB, Larson PE, Harzstark AL, Ferrone M, van Criekinge M, Chang JW, Bok R, Park I, Reed G, Carvajal L, Small EJ, Munster P, Weinberg VK, Ardenkjaer-Larsen JH, Chen AP, Hurd RE, Odegardstuen LI, Robb FJ, Tropp J, Murray JA (2013) Metabolic imaging of patients with prostate cancer using hyperpolarized [1-(1)(3)C]pyruvate. Sci Transl Med 5:198ra108
135. Gallagher FA, Woitek R, McLean MA, Gill AB, Manzano Garcia R, Provenzano E, Riemer F, Kaggie J, Chhabra A, Ursprung S, Grist JT, Daniels CJ, Zaccagna F, Laurent MC, Locke M, Hilborne S, Frary A, Torheim T, Boursnell C, Schiller A, Patterson I, Slough R, Carmo B, Kane J, Biggs H, Harrison E, Deen SS, Patterson A, Lanz T, Kingsbury Z, Ross M, Basu B, Baird R, Lomas DJ, Sala E, Wason J, Rueda OM, Chin SF, Wilkinson IB, Graves MJ, Abraham JE, Gilbert FJ, Caldas C, Brindle KM (2020) Imaging breast cancer using hyperpolarized carbon-13 MRI. Proc Natl Acad Sci USA 117:2092–2098
136. Tiwari V, Ambadipudi S, Patel AB (2013) Glutamatergic and GABAergic TCA cycle and neurotransmitter cycling fluxes in different regions of mouse brain. J Cereb Blood Flow Metab 33:1523–1531
137. Delamillieure P, Constans JM, Fernandez J, Brazo P, Benali K, Courthéoux P, Thibaut F, Petit M, Dollfus S (2002) Proton magnetic resonance spectroscopy (1H MRS) in Schizophrenia: investigation of the right and left hippocampus, thalamus, and prefrontal cortex. Schizophr Bull 28:329–339
138. Bowen BC, Pattany PM, Bradley WG, Murdoch JB, Rotta F, Younis AA, Duncan RC, Quencer RM (2000) MR imaging and localized proton spectroscopy of the precentral gyrus in amyotrophic lateral sclerosis. Am J Neuroradiol 21:647
139. Bednařík P, Moheet A, Deelchand DK, Emir UE, Eberly LE, Bareš M, Seaquist ER, Öz G (2015) Feasibility and reproducibility of neurochemical profile quantification in the human hippocampus at 3 T. NMR Biomed 28:685–693
140. Mangia S, Kumar AF, Moheet AA, Roberts RJ, Eberly LE, Seaquist ER, Tkáč I (2013) Neurochemical profile of patients with type 1 diabetes measured by 1H-MRS at 4 T. J Cereb Blood Flow Metab 33:754–759
141. Wolfgang Staffen MD, Harald Zauner PhD, Aldis Mair MD, Andrea Kutzelnigg MD, Peter Kapeller MD, Hilde Stangl MD, Edith Raffer MD, Helmut Niederhofer MD, Gunther Ladurner MD (2005) Magnetic resonance spectroscopy of memory and

frontal brain region in early multiple sclerosis. J Neuropsychiatry Clin Neurosci 17:357–363
142. Pavia DL, Lampman GM, Kriz GS (1979) Introduction to spectroscopy: a guide for students of organic chemistry. W.B. Saunders Co, Philadelphia